

THE MID-INFRARED ABSORPTION SPECTRA OF NEUTRAL POLYCYCLIC AROMATIC HYDROCARBONS IN CONDITIONS RELEVANT TO DENSE INTERSTELLAR CLOUDS

M. P. BERNSTEIN, S. A. SANDFORD, AND L. J. ALLAMANDOLA

NASA Ames Research Center, MS 245-6, Moffett Field, CA 94035; ssandford@mail.arc.nasa.gov

Received 2005 March 24; accepted 2005 June 17

ABSTRACT

Polycyclic aromatic hydrocarbons (PAHs) are common throughout the universe and are expected to be present in dense interstellar clouds. In these environments, some PAHs may be present in the gas phase, but most should be frozen into ice mantles or adsorbed onto dust grains and their spectral features are expected to be seen in *absorption*. Here we extend our previous work on the infrared spectral properties of the small PAH naphthalene ($C_{10}H_8$) in several media to include the full mid-infrared laboratory spectra of 11 other PAHs and related aromatic species frozen in H_2O ices. These include the molecules 1,2-dihydronaphthalene, anthracene, 9,10-dihydroanthracene, phenanthrene, pyrene, benzo[e]pyrene, perylene, benzo(k)fluoranthene, pentacene, benzo[ghi]perylene, and coronene. These results demonstrate that PAHs and related molecules, as a class, show the same spectral behaviors as naphthalene when incorporated into H_2O -rich matrices. When compared to the spectra of these same molecules isolated in inert matrices (e.g., Ar or N_2), the absorption bands produced when they are frozen in H_2O matrices are broader (factors of 3–10), show small position shifts in either direction (usually $<4\text{ cm}^{-1}$, always $<10\text{ cm}^{-1}$), and show variable changes in relative band strengths (typically factors of 1–3). There is no evidence of systematic increases or decreases in the absolute strengths of the bands of these molecules when they are incorporated in H_2O matrices. In H_2O -rich ices, their absorption bands are relatively insensitive to concentration over the range of $10 < H_2O/PAH < 200$. The absorption bands of these molecules are also insensitive to temperature over the $10\text{ K} < T < 125\text{ K}$ range, although the spectra can show dramatic changes as the ices are warmed through the temperature range in which amorphous H_2O ice converts to its cubic and hexagonal crystalline forms ($T > 125\text{ K}$). Given the small observed band shifts caused by H_2O , the current database of spectra from Ar matrix-isolated neutral PAHs and related molecules should be useful for the search for these species in dense clouds on the basis of observed absorption band positions. Furthermore, these data permit determination of column densities to better than a factor of 3 for PAHs in dense clouds. Column density determination of detected aromatics to better than a factor of 3 will, however, require good knowledge about the nature of the matrix in which the PAH is embedded and laboratory studies of relevant samples.

Subject headings: infrared: ISM — ISM: lines and bands — ISM: molecules — line: formation — line: identification — molecular data

1. INTRODUCTION

Polycyclic aromatic hydrocarbons (PAHs) and related aromatic materials are thought to be present in virtually all phases of the interstellar medium (ISM; Allamandola et al. 1999). Interstellar PAHs are most easily seen under conditions where gas-phase PAHs (both neutrals and ions) are excited by UV and visible light and cool through the emission of infrared (IR) photons, giving rise to the well-known emission spectra with prominent features at 3050 , 1610 , 1300 , 1160 , and 890 cm^{-1} (3.28 , 6.2 , 7.6 , 8.6 , and $11.2\text{ }\mu\text{m}$; e.g., Allamandola et al. 1989; Peeters et al. 2002). However, PAHs in dense interstellar clouds will be largely screened from exciting radiation. In addition, since dense molecular clouds are extremely cold ($T < 50\text{ K}$), most PAHs in these environments should be efficiently condensed onto dust grains, either as “pure” solids or as “guest molecules” in icy grain mantles, as is the case for most other interstellar molecules (Sandford & Allamandola 1993). The presence of PAHs in dense clouds is further suggested by the presence of aromatics in primitive meteorites and interplanetary dust particles that contain deuterium enrichments best explained by an interstellar dense cloud chemistry (Sandford 2002). Under dense cloud conditions, these PAHs will be seen in *absorption*.

Because they fall at positions characteristic of aromatic molecules, a few weak mid-infrared absorption features have been attributed to PAHs along lines of sight to a limited number of objects embedded in dense clouds. These include bands near

3030 cm^{-1} ($3.3\text{ }\mu\text{m}$; Smith et al. 1989; Sellgren et al. 1995; Brooke et al. 1999), and 1600 cm^{-1} ($6.2\text{ }\mu\text{m}$; Chiar et al. 2000), and 890 cm^{-1} ($11.2\text{ }\mu\text{m}$; Bregman et al. 2000).

Beyond making a general connection with aromatic materials, it has proven difficult to fully interpret these features, however. Although there is a growing database of laboratory IR absorption spectra of both neutral and ionized PAHs in inert gas matrices (e.g., Hudgins & Allamandola 1995a, 1995b; Szczepanski et al. 1995; Hudgins & Sandford 1998a, 1998b, 1998c; Mattioda et al. 2003; and references therein¹), these data have been taken to address the interpretation of the IR *emission* bands of interstellar *gas-phase* PAHs. However, the PAHs in dense clouds are expected to be condensed onto dust grains, largely as neutral molecules frozen in H_2O -rich ice mantles. Under these conditions, the PAHs will interact with each other and with other molecules. Because these interactions will perturb their infrared spectral properties (band positions, widths, profiles, and strengths), analyses of aromatic absorption bands in the spectra of dense clouds will require laboratory absorption spectra of appropriate analog materials taken under realistic astrophysical conditions.

Lines of sight that probe dense molecular clouds show that H_2O is the dominant ice component present (Sandford 1996; Ehrenfreund & Charnley 2000; van Dishoeck 2004). Thus, for PAHs in dense clouds, the most important molecular interaction

¹ See also <http://www.astrochem.org/pahdata/>.

to consider is that between PAHs and H₂O. H₂O is a relatively polar molecule and can interact quite strongly with other molecules in the solid state (see, e.g., Sandford et al. 1988; Ehrenfreund et al. 1998; Dartois et al. 1999; Gerakines et al. 1999). A systematic study of the infrared spectral properties of the two-ring PAH naphthalene (C₁₀H₈) demonstrated that interactions with H₂O resulted in relatively small changes in the positions and strengths of this molecule's vibrational bands, but significant changes in bandwidths (Sandford et al. 2004, hereafter SBA04). However, to date, very little work has been done on the infrared spectral properties of multiring PAHs frozen in H₂O-rich ices.

Here, we present the infrared spectra of 11 additional PAHs and related species frozen in H₂O ices. We find that PAHs, as a class, show very similar spectral effects to those observed previously for naphthalene. The experimental techniques used for this work are summarized in § 2, and the data obtained from the various H₂O-PAH systems examined are shown in § 3. These data establish generalized rules that can be applied to the absorption spectra of PAHs in dense interstellar clouds. The importance of these data for the interpretation of the infrared spectra of dense cloud lines of sight are briefly described in § 4; a more detailed discussion of the astrophysical implications of these results will be presented elsewhere (L. J. Allamandola, S. A. Sandford, & M. P. Bernstein 2005, in preparation).

2. EXPERIMENTAL TECHNIQUES

2.1. Sample Production and Spectroscopy

The work presented here expands on our early work with the PAH naphthalene (C₁₀H₈) in H₂O-rich ices (SBA04) by the addition of eight more six-membered ring PAHs [anthracene (C₁₄H₁₀), phenanthrene (C₁₄H₁₀), pyrene (C₁₆H₁₀), benzo[e]pyrene (C₂₀H₁₂), perylene (C₂₀H₁₂), pentacene (C₂₂H₁₄), benzo[ghi]perylene (C₂₂H₁₂), and coronene (C₂₄H₁₂)], the H_n-PAHs 1,2-dihydronaphthalene (C₁₀H₁₀) and 9,10-dihydroanthracene (C₁₄H₁₂; PAHs with extra peripheral H atoms), and benzo(k)fluoranthene (C₂₀H₁₂), an aromatic molecule containing a five-membered ring. The structures of these molecules are shown in the figures.

The H₂O-PAH samples studied in this paper were vapor deposited as sub-micron-thick films on a CsI window. The window was held at ~15 K and was suspended in an evacuated sample chamber at a pressure of ~10⁻⁸ torr. Detailed descriptions of the general ice deposition process and apparatus can be found elsewhere (Bernstein et al. 1995; Hudgins & Allamandola 1995a).²

The H₂O used in these experiments was purified via a Millipore Milli-Q water system to 18.2 MΩ and freeze/pump/thawed three times in vacuum to remove dissolved gases prior to use. The PAHs (obtained from the Aldrich Chemical Company unless otherwise noted) were used without further purification and were reported to have the following purities: 1,2-dihydronaphthalene (99+%), anthracene (99%), 9,10-dihydroanthracene (97%), phenanthrene (99.5+%), pyrene (Fluka; >99%), benzo[e]pyrene (99%), perylene (99+%), benzo(k)fluoranthene (Janssen Chimica; 99+%), pentacene (98%), benzo[ghi]perylene (98%), and coronene (99%).

Except for 1,2-dihydronaphthalene, all the PAHs examined in this study are solids at room temperature and have low vapor pressures. As a result, only the H₂O-dihydronaphthalene sample was deposited from a bulb premixed in the gas phase at room temperature prior to deposition, as was done in our previous study on H₂O-naphthalene samples (SBA04). For all the other samples, H₂O and the molecule under study were codeposited onto the

CsI substrate through separate inlets. The H₂O was deposited from a gas bulb containing pure H₂O vapor prepared from a liquid sample on a glass manifold with a background pressure of ~1 × 10⁻⁵ mbar. Since the pressure in the H₂O sample bulbs fell between 10 and 20 mbar, the contaminant levels associated with the H₂O were negligible. The flow rate of H₂O onto the cold window was controlled by a microflowmeter.

The PAHs were sublimed from a pyrex tube wrapped in resistive heating wire and mated to the sample chamber (see Hudgins & Allamandola 1995a). The tube was heated to different temperatures, depending on the vaporization point of the PAH in question. The temperatures used were anthracene (60°C), 9,10-dihydroanthracene (60°C), phenanthrene (23°C), pyrene (60°C), benzo[e]pyrene (120°C), perylene (165°C), benzo(k)fluoranthene (130°C), pentacene (220°C), benzo[ghi]perylene (150°C), and coronene (160°C). Different H₂O/PAH ratios were achieved by varying the H₂O flow rate and/or slightly varying the heat of the PAH sample upward or downward.

The H₂O-PAH sample gases were typically codeposited onto the 15 K CsI window at a rate that produced an ~0.1 μm thick ice layer after a few minutes of deposition. This deposition technique produces an ice composed of an intimate mixture of the PAH molecules in amorphous H₂O, the form of H₂O ice believed to be found in interstellar molecular clouds (Allamandola & Sandford 1988; Jenniskens & Blake 1994; Jenniskens et al. 1995). The PAH sample tube typically takes several minutes to come up to the proper sublimation temperature, and during this time the rate of sublimation varies. In addition, the flow of H₂O vapor may take as much as several minutes to come up to its maximum rate of flow after deposition begins. In order to maintain steady relative deposition rates for the studied samples, all depositions were begun with the sample window in a position shielded from the sample inlets and it was only turned to face the deposition ports after the PAH temperature and the H₂O flow rate stabilized. Similarly, the sample deposition was halted by shutting off the flows of sample materials and rotating the sample substrate to the shielded position. The H₂O-1,2-dihydronaphthalene sample was simply deposited on the cold window directly from the premixed sample bulb.

After deposition onto the CsI window, the 4000–500 cm⁻¹ (2.5–20 μm) infrared spectrum of each sample was measured at a resolution of 0.9 cm⁻¹ (the observed width of an unresolved line) and ratioed to a spectrum taken previously of the blank cold window, resulting in a standard transmission spectrum. Analyses of the areas of the infrared absorption bands of both the H₂O and PAHs in the spectra verified that our sample ice layers had thicknesses of a few tenths of a micron. In some cases, additional spectra were also measured after the samples had been warmed to temperatures of 25, 50, 75, 100, 125, 150, and 175 K. Samples were warmed at a rate of ~2 K per minute between the temperature steps and were allowed to equilibrate for 5 minutes at each temperature before spectra were taken.

2.2. H₂O/PAH Sample Ratios

In our previous work with H₂O-naphthalene, it was possible to carefully control the H₂O/C₁₀H₈ ratios of the samples since both species could be premixed in the gas phase. Since all but one of the more refractory PAHs considered in this work have vapor pressures that are too low to allow for predeposition, gas phase mixing, we had to use parallel deposition (§ 2.1), making it difficult to precisely control the ultimate H₂O/PAH ratios of our samples. Since H₂O/PAH ratios so far observed in the ISM seems to lie somewhere between 5 and 200 (SBA04 and references therein), we targeted the production of samples having H₂O/PAH ratios in

² See also <http://www.astrochemistry.org>.

this range. Under these conditions, the PAHs in the ice are not all fully isolated from each other (Behringer 1958). At the most concentrated end of this range less than 50% of the PAHs will be monomeric, i.e., fully surrounded by H₂O molecules; the rest will reside in PAH dimers, trimers, and higher multimers. At the more dilute end of the range, as much as ~90% of the PAHs in an ice may be fully isolated, with most of the rest of the PAHs being present as dimers. Thus, while these samples span a range of concentrations, both H₂O-PAH and PAH-PAH interactions may play important roles in defining the infrared spectra of all the samples.

Since most of our H₂O-PAH samples could not be premixed prior to deposition, it was necessary to estimate the H₂O/PAH ratio of each sample after deposition was complete. This was done by determining the relative column densities of H₂O and PAH in the infrared beam in the final sample. The column density of H₂O was determined by measuring the band areas of the O-H stretching mode (3300 cm⁻¹; 3.0 μm) and H-O-H bending mode (1660 cm⁻¹; 6.0 μm) bands of H₂O ice and assuming band strengths of 1.7 × 10⁻¹⁶ and 1.0 × 10⁻¹⁷ cm per molecule, respectively (Hudgins et al. 1993). The column density of the given PAH in a sample was estimated by measuring the areas of multiple bands of the PAH and using their calculated band strengths. For most of our samples we used calculated absolute band strengths published for the relevant modes of isolated PAHs (Langhoff 1996; Hudgins & Sandford 1998a, 1998b, 1998c; Sandford et al. 2004). For the two H_n-PAHs, we used newly calculated values (C. Bauschlicher 2003, unpublished).

Our previous work on the H₂O-naphthalene system demonstrated that H₂O produces modest changes in the relative band strengths of the guest naphthalene. However, on average, the relative band strengths of the various naphthalene modes were consistent with Ar matrix data to within ~50%, implying that calculated band strengths for individual bands were good to better than a factor of 2–3 (SBA04). There was no evidence that the presence of H₂O caused either systematic increases or decreases in the strengths of the C₁₀H₈ absorption bands as a whole. Assuming the same holds true for the molecules studied here, an estimate of the H₂O/PAH ratios in our samples can be obtained by averaging the PAH column densities derived from multiple bands from each PAH. We typically averaged column densities from 5 to 10 bands to estimate the H₂O/PAH ratios reported here. Thus, assuming the PAHs discussed here behave similarly to naphthalene, the H₂O/PAH ratios reported here are probably accurate to better than a factor of 2.

Using this process we derived the following H₂O/PAH ratios: H₂O/1,2-dihydronaphthalene ≈ 20 and 50, H₂O/anthracene ≈ 70, H₂O/9,10-dihydroanthracene ≈ 50, H₂O/phenanthrene ≈ 200, H₂O/pyrene ≈ 10 and 380, H₂O/benzo[e]pyrene ≈ 35, H₂O/perylene ≈ 40, H₂O/benzo(k)fluoranthene ≈ 100, H₂O/pentacene ≈ 75, H₂O/benzo[ghi]perylene ≈ 130, and H₂O/coronene ≈ 40 and 160. Thus, all our samples have PAH concentrations in the 0.3%–10% range, with the majority falling in the 1%–3% range.

3. RESULTS

3.1. The IR Spectra of PAHs in H₂O-rich Ices

As previously demonstrated for H₂O-naphthalene ices (SBA04), the mid-infrared spectra (4000–500 cm⁻¹; 2.5–20 μm) of PAHs frozen in H₂O-rich samples are dominated by the strong vibrational modes of H₂O, even in H₂O ices containing concentrations of PAHs that are much higher than considered to be astrophysically relevant. Figure 1 shows the full mid-infrared spectrum of an H₂O/pyrene ≈ 10 sample at 15 K, the sample with the highest concentration of PAH relative to H₂O of any of the samples we

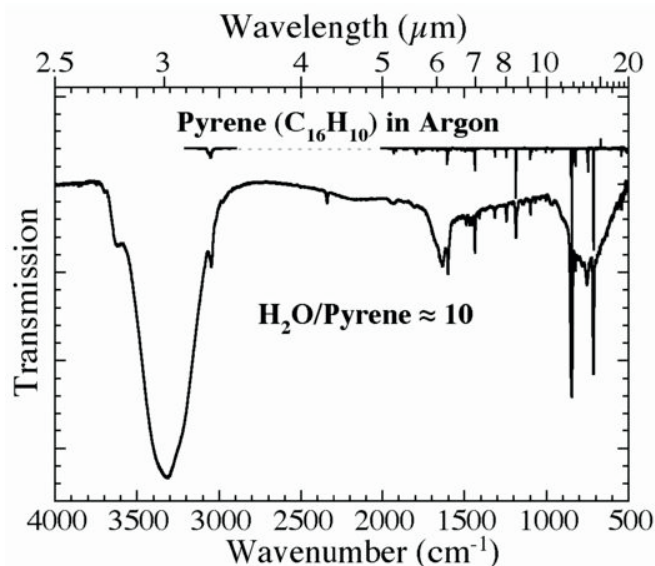


FIG. 1.—Plot of the 4000–500 cm⁻¹ (2.5–20 μm) infrared spectra of pyrene (C₁₆H₁₀) isolated in an argon matrix at 12 K (Ar/C₁₆H₁₀ > 1000; from Hudgins & Sandford 1998a) (top) and in an H₂O matrix (H₂O/C₁₆H₁₀ ≈ 10) at 15 K (bottom). The Ar and H₂O spectra are offset vertically for clarity. The H₂O-pyrene spectrum is dominated by the H₂O features at 3320, 1630, and 750 cm⁻¹ (3.0, 6.1, and 13.3 μm) but also shows features associated with the fundamental vibrations of pyrene and an enhanced dangling O-H band near 3620 cm⁻¹ (2.76 μm).

discuss in this paper, compared with the spectrum of pyrene isolated in an Ar matrix.

The most prominent features in the H₂O-pyrene spectrum are those of the O-H stretch, H-O-H bend, and librational modes of H₂O near 3320, 1630, and 750 cm⁻¹ (3.0, 6.1, and 13.3 μm), respectively. The presence of the pyrene produces additional, weaker bands in the spectrum. The majority of these absorptions are associated with the fundamental vibrational modes of pyrene itself, as evidenced by the match of these bands to the infrared spectrum of pyrene isolated in argon. As will be shown in subsequent figures, these bands are generally very weak relative to those of H₂O in samples with H₂O/PAH > 20.

Additional bands are also generally seen in the 3750–3600 cm⁻¹ (2.67–2.78 μm) region. These features are due to “dangling O-H groups,” i.e., hydrogen atoms in H₂O molecules in the ice structure that are not H-bonded with a neighboring H₂O molecule. This feature is weak in the spectra of pure H₂O ice, but it is commonly larger in the spectra of H₂O ices that contain non-H-bonding guest molecules that interfere with the H-bonding network (Rowland & Devlin 1991; Rowland et al. 1991; SBA04). The increased strength of these bands in our spectra are a clear indication that the PAHs in our samples partially disrupt the H-bonding network of the H₂O ice and that they are intimately mixed within the H₂O matrix.

For most of the samples described here (PAHs, H_n-PAHs, and fluoranthene), these dangling OH groups produce two weak features near 3720 and 3695 cm⁻¹ (2.69 and 2.71 μm), with the 3695 cm⁻¹ feature being approximately twice as strong as the 3720 cm⁻¹ feature. The strengths of these bands increase with increasing concentration of the guest molecule, and at the very highest concentrations (see Fig. 1) can result in shifts in the band positions. While the presence of the PAHs in our samples are responsible for these bands, similar effects are seen when many other molecular species are incorporated into H₂O ices. Thus, while these features are expected to be present in the spectra of PAH-containing ices, they cannot be considered to be diagnostic

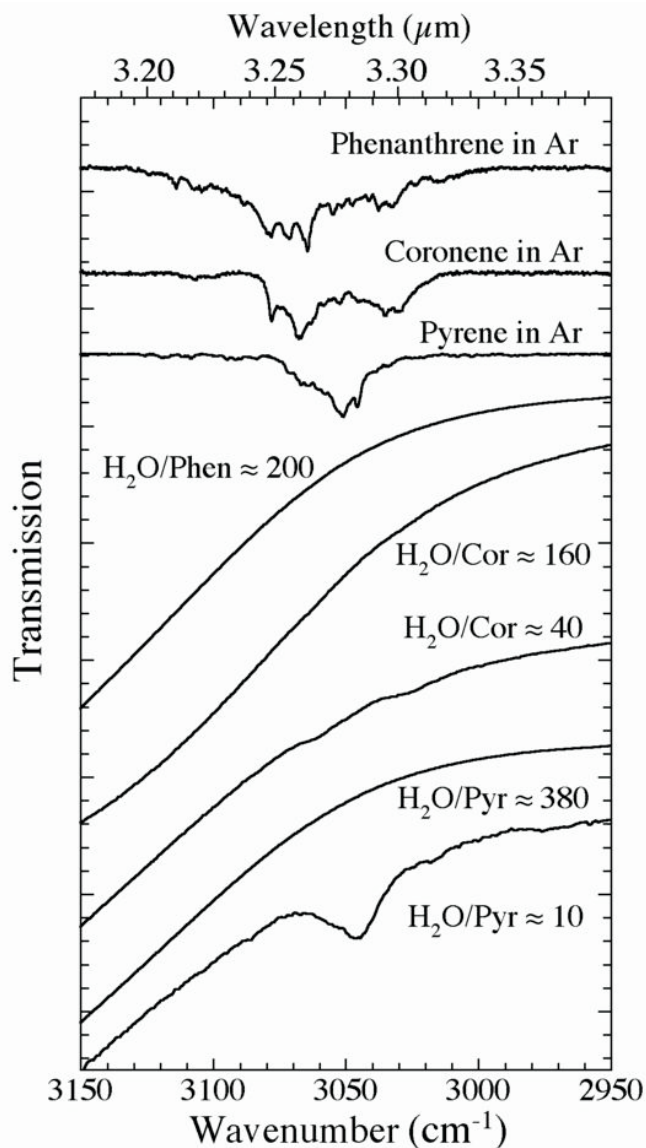


FIG. 2.—Plot of the $3150\text{--}2950\text{ cm}^{-1}$ ($3.17\text{--}3.39\text{ }\mu\text{m}$) spectra of phenanthrene, coronene, and pyrene in Ar and H_2O matrices. The spectra are offset vertically for clarity. The H_2O -PAH spectra span a range of PAH concentrations and demonstrate how the presence of the nearby H_2O band suppresses the spectral contrast of these vibrational modes. As with naphthalene, the C-H stretching bands of other PAHs only become weakly visible as the H_2O /PAH ratio falls below ~ 50 , i.e., PAH concentrations in the H_2O exceed a few percent.

of the presence of PAHs per se, but rather indicate only that some molecules other than H_2O are present in the H_2O ice.

3.2. The Absorption Spectra of PAHs in H_2O Matrices

The infrared spectra of our H_2O -PAH samples are shown in Figures 2, 3, 4, 5, 6, and 7. These mixtures span the range of PAH concentrations likely to be observable in astronomical ices (SBA04). For comparison, spectra are also shown for each PAH isolated in an Ar matrix. Tables 1, 2, and 3 provide lists of the strongest PAH bands in the spectra of the H_2O -PAH mixtures examined. Relative band strengths are all normalized to the strongest band in the C-H out-of-plane bending mode region. The tables list all bands having relative strengths of 10% or greater and a minimum of the five strongest PAH bands present, independent of relative strength.

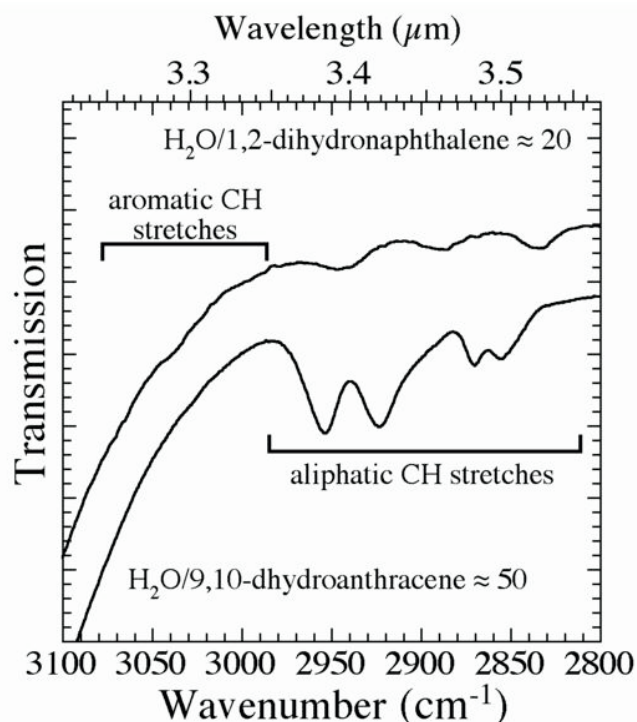


FIG. 3.—Plot of the $3100\text{--}2800\text{ cm}^{-1}$ ($3.23\text{--}3.57\text{ }\mu\text{m}$) spectra of 1,2-dihydronaphthalene and 9,10-dihydroanthracene in H_2O matrices ($\text{H}_2\text{O}/1,2$ -dihydronaphthalene ≈ 20 and $\text{H}_2\text{O}/9,10$ -dihydroanthracene ≈ 50). The spectra are offset vertically for clarity. The structures for these two molecules can be seen in Figs. 4b and 4d. The regions in which aromatic and aliphatic CH stretching vibrations fall are marked with horizontal bars. While the aromatic CH stretching bands of these molecule are barely visible at these concentrations, the aliphatic CH stretching bands are readily apparent.

3.2.1. The C-H Stretching Band of PAHs in H_2O -rich Ices

Since the aromatic C-H stretching bands of all PAHs fall in the vicinity of 3030 cm^{-1} ($3.3\text{ }\mu\text{m}$), they are always severely blended with the strong, broad O-H stretch of H_2O when in H_2O -rich ices. Thus, as with the H_2O -naphthalene system, it is difficult to measure the precise positions, widths, and especially strengths, of the various PAHs' aromatic C-H stretching features in the $3150\text{--}2980\text{ cm}^{-1}$ ($3.17\text{--}3.36\text{ }\mu\text{m}$) region unless the PAH is present in very high concentrations. This is largely because of the underlying concave, long-wavelength shoulder of the overlapping H_2O band. The changing slope imposed by the H_2O makes it difficult to define the baselines underlying the features and suppresses their apparent strengths. This effect is exacerbated by interactions with the H_2O matrix that increase the width of these absorption features, further decreasing their spectral contrast. The result is that the aromatic C-H stretching modes are significantly masked when PAHs are placed in an H_2O ice. Figure 2 shows this spectral region for several of our H_2O -PAH samples that span the range from our lowest PAH concentrations to our highest. No features are apparent at our lowest concentrations, and they only begin to become apparent when the PAH concentration exceeds a few percent that of the H_2O in the matrix. Clearly, straight baselines drawn under such features will always *underestimate* the true strength of the aromatic C-H stretching bands.

The individual features can be partially "recovered" if the spectra of pure H_2O ices are used to partially subtract out the underlying slope of the $3\text{ }\mu\text{m}$ H_2O feature, but such corrections are imperfect since the profile of this feature is temperature

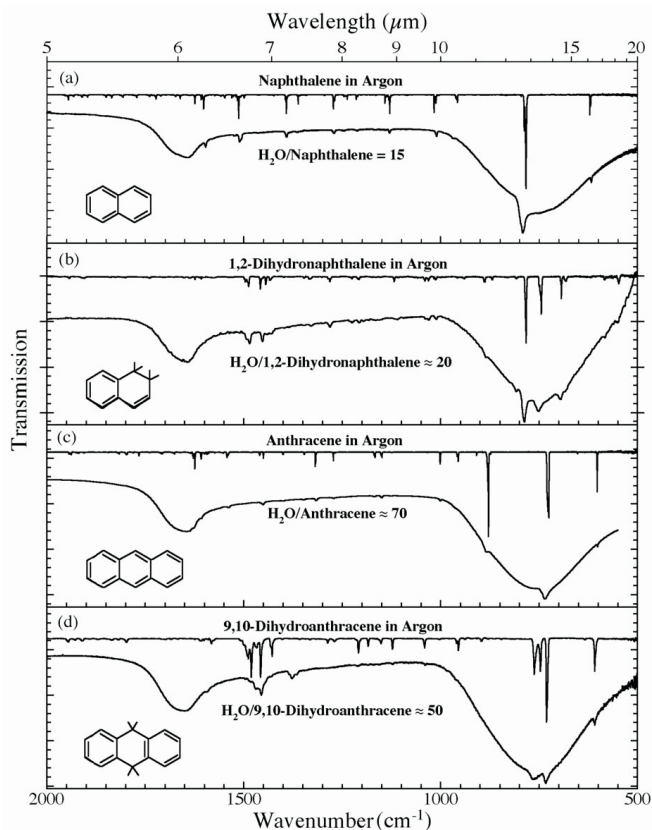


FIG. 4.—Plot of the 2000–500 cm^{-1} (5.0–20.0 μm) infrared spectra of (a) H_2O /naphthalene ≈ 15 , (b) H_2O /1,2-dihydronaphthalene ≈ 20 , (c) H_2O /anthracene ≈ 70 , and (d) H_2O /9,10-dihydroanthracene ≈ 50 . Each H_2O /PAH spectrum is compared to the spectrum of the relevant PAH isolated in an Ar matrix. The Ar and H_2O spectra are offset vertically for clarity. The Ar matrix data for naphthalene and anthracene were taken from Hudgins & Sandford (1998a). The Ar matrix data for 1,2-dihydronaphthalene and 9,10-dihydroanthracene are taken from S. A. Sandford et al. (2006, in preparation). All spectra were measured from samples at 15 K. Positions, widths, and relative strengths of the strongest PAH bands in these spectra are summarized in Table 1.

dependent and is affected by the presence of other molecular species (including the guest PAH molecules themselves). As was the case for naphthalene, we see no evidence that the presence of the H_2O causes a significant change in the overall strength of the C–H stretching mode; it simply “hides” it (see SBA04 for a more detailed discussion). This seems to hold true for all the *aromatic* CH stretching bands we have examined, whether they be in a PAH, H_n -PAH, or fluoranthene.

It should be noted, however, that the *aliphatic* C–H stretching features of H_n -PAHs provide greater spectral contrast than observed for the purely *aromatic* CH stretches of both normal PAHs and H_n -PAHs. The presence of extra peripheral hydrogen atoms in H_n -PAHs converts some of the peripheral aromatic carbons (–C–H) into aliphatic carbons (– CH_2 – groups), thereby generating rings that have aliphatic, or partially aliphatic, character (Bernstein et al. 1996). The C–H stretching modes of these aliphatic groups typically fall between 2980 and 2800 cm^{-1} (3.36–3.57 μm) and can show considerably stronger spectral contrast in H_2O than do the aromatic C–H stretching bands. Figure 3 shows the examples of 1,2-dihydronaphthalene and 9,10-dihydroanthracene where the more abundant aromatic stretches of CH groups (6 and 8 C–H bonds, respectively) are barely visible at concentrations of 2%–5%, while the features due to the two – CH_2 – groups (four C–H bonds) in each molecule show considerably better spectral contrast (see also Table 1). This in-

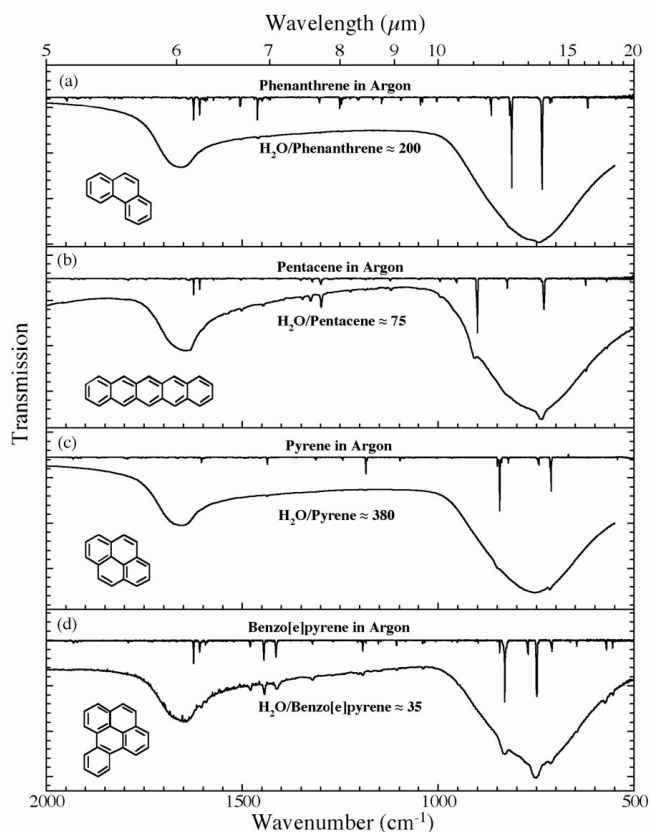


FIG. 5.—Plot of the 2000–500 cm^{-1} (5.0–20.0 μm) infrared spectra of (a) H_2O /phenanthrene ≈ 200 , (b) H_2O /pentacene ≈ 75 , (c) H_2O /pyrene ≈ 380 , and (d) H_2O /benzo[e]pyrene ≈ 35 . Each H_2O /PAH spectrum is compared to the spectrum of the relevant PAH isolated in an Ar matrix. The Ar and H_2O spectra are offset vertically for clarity. The Ar matrix data for phenanthrene and pyrene are taken from Hudgins & Sandford (1998a); those for pentacene and benzo[e]pyrene are taken from Hudgins & Sandford (1998b). All spectra were measured from samples at 15 K. Positions, widths, and relative strengths of the strongest PAH bands in these spectra are summarized in Table 2.

creased contrast for the aliphatic CH stretching modes is due to several effects. First, since they lie at lower frequencies than the aromatic CH stretches, these features fall further out on the wing of the 3 μm H_2O feature and suffer considerably less baseline distortion. Second, these modes tend to produce proportionally stronger features because they contain twice as many CH modes per carbon and the intrinsic oscillator strength per CH bond is 2–3 times greater for aliphatics than aromatics.

The exact positions and strengths of the aliphatic CH stretches of H_n -PAHs are very sensitive to the degree of excess H coverage and to the specific location of the extra H atoms (C. Bauschlicher 2003, unpublished), as evidenced by the very different aliphatic CH stretching absorption profiles of the two molecules in Figure 3. This may have interesting implications for the long-wavelength wing seen on the 3 μm ice band in many dense cloud spectra (see § 4; L. J. Allamandola, S. A. Sandford, & M. P. Bernstein 2005, in preparation).

3.2.2. The Positions and Widths of Other PAH Bands in H_2O -PAH Samples

Overall, the 2000–500 cm^{-1} (5–20 μm) absorption spectra of all our samples show behaviors that are very similar to those observed for the H_2O -naphthalene system (compare Figs. 4–7 with those of SBA04). Peak positions show only modest shifts compared to those observed when the same molecules are isolated in

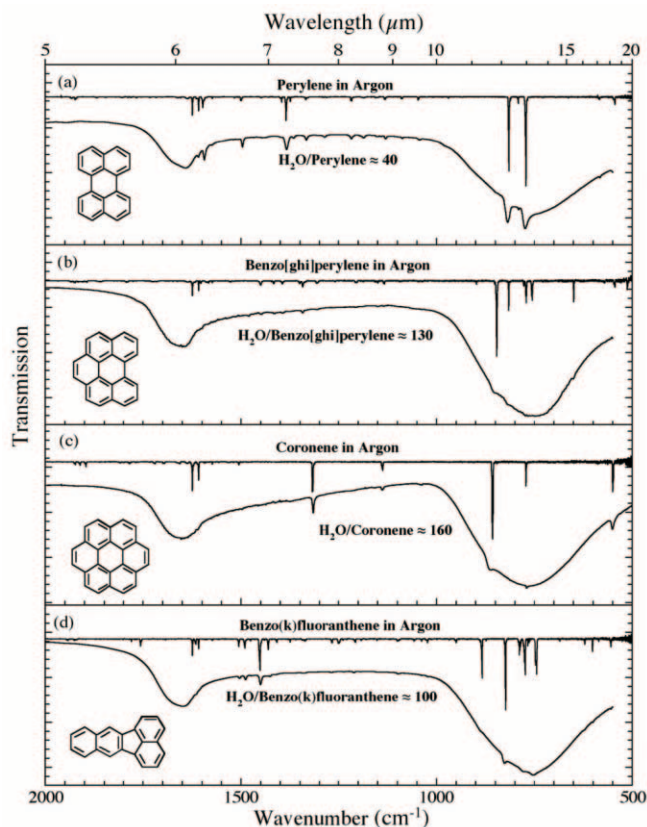


FIG. 6.—Plot of the 2000–500 cm^{-1} (5.0–20.0 μm) infrared spectra of (a) H_2O /perylene ≈ 40 , (b) H_2O /benzo[ghi]perylene ≈ 130 , (c) H_2O /coronene ≈ 160 , and (d) H_2O /benzo(k)fluoranthene ≈ 100 . Each H_2O /PAH spectrum is compared to the spectrum of the relevant PAH isolated in an Ar matrix. The Ar and H_2O spectra are offset vertically for clarity. The Ar matrix data for perylene, benzo[ghi]perylene, and coronene are taken from Hudgins & Sandford (1998b); the spectrum of benzo(k)fluoranthene are taken from Hudgins & Sandford (1998c). All spectra were measured from samples at 15 K. Positions, widths, and relative strengths of the strongest PAH bands in these spectra are summarized in Table 3.

Ar. Observed band shifts are typically less than 4 cm^{-1} , are everywhere $< 10 \text{ cm}^{-1}$, and can be either upward or downward in frequency. The largest shifts ($5\text{--}10 \text{ cm}^{-1}$) frequently involve C-H out-of-plane bending vibrations that generally fall in the $900\text{--}750 \text{ cm}^{-1}$ ($11.1\text{--}13.3 \mu\text{m}$) range. However, this effect is not universal; approximately half of the species examined show only the normal ($< 4 \text{ cm}^{-1}$) shifts in their out-of-plane bending modes (9,10-dihydroanthracene, pyrene, benzo[e]pyrene, perylene, and coronene). Where they occur, large out-of-plane bending mode position shifts are always blueshifts, i.e., shifts to higher frequency. Where different concentrations have been studied, it appears that the band shifts are relatively insensitive to concentration. All these shifts are interpreted as being due to H_2O -PAH and PAH-PAH interactions. This interpretation is consistent with our observations of the quinoline- H_2O system, where stronger interactions produce bigger changes in the spectra (Bernstein et al. 2005).

The observed bandwidths for our various H_2O -PAH samples are also similar to those observed for the H_2O -naphthalene system—typically being 3–10 times those observed for the same PAHs in inert Ar matrices. Features in the $2000\text{--}1000 \text{ cm}^{-1}$ ($5\text{--}10 \mu\text{m}$) range are typically $4\text{--}8 \text{ cm}^{-1}$ wide, although both narrower and broader features are seen on occasion. Broader bands are frequently due to the overlap of nearby features. Features in the $1000\text{--}500 \text{ cm}^{-1}$ ($10\text{--}20 \mu\text{m}$) range are broader, on average,

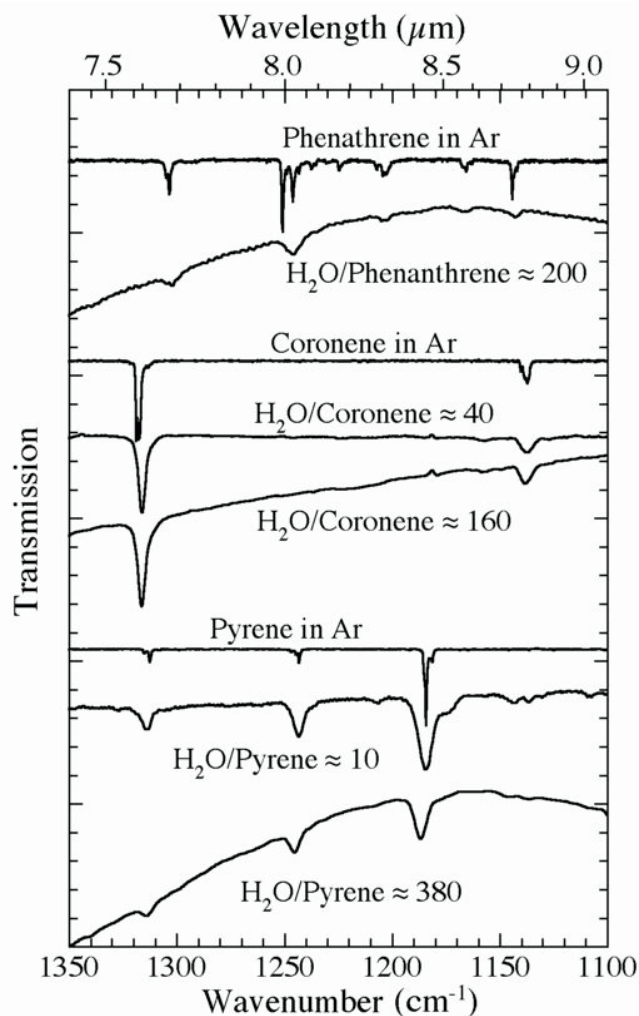


FIG. 7.—Plot of the $1350\text{--}1100 \text{ cm}^{-1}$ ($7.41\text{--}9.1 \mu\text{m}$) infrared spectra of several PAHs frozen in Ar and in H_2O -rich ices at different concentrations. The spectra are offset vertically for clarity. Compared to their spectra when isolated in Ar, the absorption bands of PAHs in H_2O ices generally show increased widths but only modest shifts in position and relative band strengths. The magnitude of these changes is largely independent of concentration over the range considered here. All spectra were taken from samples deposited and maintained at 15 K.

than higher frequency bands, with $10\text{--}20 \text{ cm}^{-1}$ widths being fairly common. However, as with the higher frequency modes, bands as narrow as $2\text{--}3 \text{ cm}^{-1}$ are still occasionally seen. As with the H_2O -naphthalene system, these increased widths are interpreted as being due to H_2O -PAH interactions and the presence of a distribution of PAH site geometries within the amorphous H_2O ice matrix. As with peak positions, bandwidths appear to be fairly insensitive to concentration in the H_2O .

The single largest deviation we see between the Ar and H_2O matrix data occurs for 9,10-dihydroanthracene (Fig. 4d), where moderately strong absorption is seen near 1377 cm^{-1} ($7.262 \mu\text{m}$) when the molecule is frozen in H_2O but is not seen when the molecule is isolated in Ar. A strong band is not anticipated at this position on the basis of theoretical calculations (C. Bauschlicher 2003, unpublished). However, it is interesting to note that the two main CH deformation modes of aliphatic compounds generally fall near 1470 and 1370 cm^{-1} (6.8 and $7.3 \mu\text{m}$). This suggests that the 1377 cm^{-1} feature may be due to a CH deformation mode that involves little or no change in dipole moment in isolation, but

TABLE 1
 BAND POSITIONS, WIDTHS, AND RELATIVE STRENGTHS OF NAPHTHALENE, 1, 2-DIHYDROANPHTHALENE,
 ANTHRACENE, AND 9, 10-DIHYDROANTHRACENE IN H₂O MATRICES

PAH	H ₂ O/PAH Ratio	Band Position ^a (cm ⁻¹)	Bandwidth (FWHM) (cm ⁻¹)	Relative Strength ^b
Naphthalene ^c	8	617.8	2.7	0.03
		791.5	14.1	1.00
		1010.4	4.3	0.04
		1129.6	4.8	0.04
		1271.0	6.5	0.04
		1391.4	5.6	0.07
		1510.1*	8.0	0.11
		1596.7	4.1	0.05
Naphthalene ^c	15	~3055, ~3071	~12, ~5	~0.4
		618.0	2.8	0.04
		791.2	16.1	1.00
		1010.7	4.3	0.05
		1129.9	4.4	0.04
		1270.9	6.3	0.04
		1391.3	5.5	0.07
		1510.7, 1506.9	8.0	0.12
Naphthalene ^c	40	1597.2	4.3	0.05
		~3055, ~3071	~10, ~5	~0.4
		617.8	~3	0.02
		791.3	15.5	1.00
		1011.1	4.0	0.03
		1130.1	3.4	0.03
		1271.3	6.0	0.03
		1391.8	4.7	0.08
1,2-dihydronaphthalene.....	20	1510.9	7.2	0.09
		1597.8	4.3	0.03
		3060?, 3071?
		550.0	~5	0.18
		695.6*	9.4	0.18
		751.6	17.8	0.47
		788.0	10.3	1.00
		1452.7	5.4	0.13
1,2-dihydronaphthalene.....	50	1485.3*	12.9	0.39
		2834.7	20.0	0.46
		2887.7*	19.7	0.29
		2946.7*	25.8	0.47
		~3040
		549.0	5.1	0.18
		694.4	5.0	0.12
		751.2	12.8	0.46
Anthracene	70	787.3	9.7	1.00
		1452.7	6.4	0.19
		1484.7*	13.3	0.35
		2832.7*	18.4	0.43
		2889.7	20.1	0.29
		2943.0	26.0	0.50
		~3040
		601.9	3.3	0.07
Anthracene	70	735.2	17.1	1.00
		883.3	9.2	0.26
		1149.8	5.1	0.07
		1316.3	5.3	0.08
		1451.1	6.3	0.10
		1539.0	5.5	0.06
~3060?		

TABLE 1—Continued

PAH	H ₂ O/PAH Ratio	Band Position ^a (cm ⁻¹)	Bandwidth (FWHM) (cm ⁻¹)	Relative Strength ^b
9,10-dihydroanthracene.....	50	608.6	4.6	0.29
		733.9	10.7	1.00
		764.2	22.0	0.88
		1377.1*	12.4	0.64
		1456.4*	26.3	3.04
		2870.0, 2855.5	~10, ~20	85
		2953.9, 2923.3 ^d	23.4, 27.8	190
		

NOTE.—Table lists the five strongest bands in the spectrum of each PAH and all bands that have measurable strengths greater than 10%, that of the strongest band in the spectrum.

^a An asterisk (*) indicates that this is the position of the strongest feature of several overlapping bands whose combined area are provided in the final column of this table.

^b All band areas are normalized against the area of the strongest C-H out-of-plane bending band in the spectrum.

^c For a more complete listing of bands, see Sandford et al. (2004).

^d Some or all of expected aromatic CH stretching features not apparent on the wing of the H₂O feature at this concentration.

TABLE 2
BAND POSITIONS, WIDTHS, AND RELATIVE STRENGTHS OF PHENANTHRENE, PENTACENE, PYRENE,
AND BENZO[E]PYRENE IN H₂O MATRICES

PAH	H ₂ O/PAH Ratio	Band Position ^a (cm ⁻¹)	Bandwidth (FWHM) (cm ⁻¹)	Relative Strength ^b
Phenanthrene.....	200	744.0	18.2	1.00
		820.0	14.3	0.84
		1245.8	7.1	0.09
		1458.9	5.5	0.19
		1503.0	3.3	0.10
		^c
Pentacene.....	75	737.0	15.3	1.00
		906.5	15.6	0.18
		1299.3	4.0	0.23
		1325.5	5.5	0.11
		1502.2	5.2	0.06
		~3055?
Pyrene.....	10	712.4	7.9	0.42
		751.2	15.2	0.16
		844.8	14.1	1.00
		1184.4*	7.7	0.15
		1243.3	5.5	0.05
		1434.6	5.3	0.09
		1600.2	10.2	0.17
Pyrene.....	380	3046.0	19.4	0.25
		715.2	6.5	~0.6 ^d
		~754	~7?	
		848.1	10.8	1.00
		1186.6	6.4	0.11
		1245.5	4.9	0.06
		1436.5	5.5	0.15
	~1601 ^c	~8	...	
		
Benzo[e]pyrene.....	35	573.3	7.9	0.13
		711.9	11.0	0.21
		751.4	21.1	1.00
		830.7	14.5	0.52
		1320.3	8.2	0.12
		1411.6	10.3	0.25
		1443.8	5.3	0.15
		1478.4	5.3	0.10
	~3055	

NOTE.—Table lists the five strongest bands in the spectrum of each PAH and all bands that have measurable strengths greater than 10%, that of the strongest band in the spectrum.

^a An asterisk (*) indicates that this is the position of the strongest feature of several overlapping bands whose combined area are provided in the final column of this table.

^b All band areas are normalized against the area of the strongest C-H out-of-plane bending band in the spectrum.

^c Some or all of expected aromatic CH stretching features not apparent on the wing of the H₂O feature at this concentration.

^d This band falls precisely at the bottom of the H₂O libration band, and it is difficult to establish its precise position, width, or strength.

TABLE 3
BAND POSITIONS, WIDTHS, AND RELATIVE STRENGTHS OF PERYLENE, BENZO[GHI]PERYLENE, CORONENE,
AND BENZO(K)FLUORANTHENE IN H₂O MATRICES

PAH	H ₂ O/PAH Ratio	Band Position ^a (cm ⁻¹)	Bandwidth (FWHM) (cm ⁻¹)	Relative Strength ^b
Perylene.....	40	774.1	12.9	1.00
		818.4	12.0	0.89
		1217.0	6.3	0.09
		1384.1	8.9	0.36
		1496.5	4.6	0.12
		1593.9	5.1	0.18
Benzo[ghi]perylene.....	130	~3060
		651.2	6.3	0.21
		820	10.3	~0.15
		850.5	18.1	1.00
		1306.3	7.6	0.09
		1343.2	4.8	0.16
		1394.2	6.1	0.09
		1415.2	4.7	0.09
		1449.1	7.4	0.14
1480.5	5.5	0.10		
Coronene.....	40	^c
		549.6	7.0	0.39
		769.6	4.2	0.05
		860.7	18.6	1.00
		1137.1	7.3	0.08
		1315.9	4.0	0.29
Coronene.....	160	~3025	~13	~0.04
		~3062*	~14	~0.04
		550.7	7.3	0.48
		770.0	3.3	0.07
		865.2	15.3	1.00
		1138.3	5.8	0.08
Benzo(k)fluoranthene.....	100	1316.1	4.5	0.37
		~3025?
		753.2	16.7	~0.85
		777.9	10.6	0.36
		826.8	9.1	1.00
		1098.4*	6.3	0.12
Benzo(k)fluoranthene.....	100	1450.5	6.0	0.88
		1488.7	5.2	0.33
		1503.9	4.8	0.17
		^c

NOTE.—Table lists the five strongest bands in the spectrum of each PAH and all bands that have measurable strengths greater than 10%, that of the strongest band in the spectrum.

^a An asterisk (*) indicates that this is the position of the strongest feature of several overlapping bands whose combined area are provided in the final column of this table.

^b All band areas are normalized against the area of the strongest C-H out-of-plane bending band in the spectrum.

^c Some or all of expected aromatic CH stretching features not apparent on the wing of the H₂O feature at this concentration.

that is perturbed into activity by the H₂O matrix. This relatively unique behavior may be related to the fact that the tetrahedral carbons in the middle ring of 9,10-dihydroanthracene produce two different stable configurations of this molecule, one in which both end groups are tipped in the same direction (like the wings on a butterfly) and one in which the central ring is twisted. While the detailed cause of this difference in infrared activity between the H₂O and Ar matrices is not yet understood, it does serve as an indicator that, at least for the aliphatic deformation modes of H_n-PAHs, there may occasionally be departures from the general behaviors described above.

3.2.3. The Relative and Absolute Band Strengths of PAHs in H₂O Ices

As was seen in our previous studies of the H₂O-naphthalene system (SBA04), the relative band areas of these PAHs trapped

in H₂O only differ from those of the same PAHs isolated in Ar matrices by fairly modest amounts. Relative band strengths generally lie within a factor of 3 of the values observed for the same PAHs isolated in Ar and are typically within a factor of 2. As with the H₂O-naphthalene system, this indicates that H₂O-PAH and PAH-PAH interactions are causing modest changes in the absolute strengths of the PAHs' various vibrational modes. Relative band strengths for the stronger PAH bands in each spectrum can be found in Tables 1–3.

In our earlier work on the H₂O-naphthalene system, it was possible to constrain the *absolute* band strengths of the various naphthalene vibrational modes because we had accurate knowledge of the H₂O/naphthalene ratios in our samples (SBA04). In this case we demonstrated that *relative* band strengths did differ between H₂O and Ar matrix data and calculations, indicating that

individual band strengths could increase or decrease by up to factors of 2–3. However, there was no evidence, within our uncertainties, that the absolute strengths of the $C_{10}H_8$ absorptions are *systematically* strengthened or weakened by the presence of the H_2O matrix. In other words, the presence of H_2O induces modest changes in the absolute strengths of the various $C_{10}H_8$ bands, and these changes can be either upward or downward, depending on the feature, but overall, there is little systematic increase or decrease in the band strengths (perhaps none). These results indicate that calculated gas-phase naphthalene band strengths (i.e., Langhoff 1996 and Bauschlicher & Langhoff 1997) could be used to derive column densities from relevant individual astronomical features and should be accurate to within factors of 2–3, depending on the band. The measurement of multiple absorption features and/or the availability of relevant laboratory data would decrease this uncertainty.

Unfortunately, for species other than naphthalene, our inability to produce H_2O -PAH samples with predetermined concentrations precludes us from determining absolute strengths for the PAH bands we observe. Indeed, the H_2O /PAH ratios we report throughout this paper are based on the *assumption* that the *calculated* absolute strengths for the various PAH bands are, on average, correct. However, the great similarity, in all aspects, of the spectral behavior all the other H_2O -PAH systems we have studied with those of the H_2O -naphthalene systems suggests that this assumption is probably a reasonable one. Certainly, we have found no evidence that the absolute band strengths of PAHs in H_2O matrices differ systematically from those in Ar matrices.

3.3. The Effects of Concentration on the Spectra of H_2O -PAH Ices

The positions, widths, and relative strengths of the bands of naphthalene in H_2O - $C_{10}H_8$ ices were found to be quite insensitive to concentration over the range of $H_2O/C_{10}H_8 = 8$ –80 (SBA04). Although we have not carried out extensive concentration studies for all the H_2O -PAH systems described here, it is clear that the spectra of other PAHs frozen in H_2O -rich ices show a similarly weak dependence on concentration, at least in the cases studied here. Figure 7 and Tables 1–3 show comparisons between a portion of the spectra of several PAHs in both Ar and H_2O matrices, with the H_2O /PAH ratios spanning the entire range studied here. In all cases, the H_2O -PAH samples produce PAH absorption features with similar band positions, widths, and relative strengths.

A threshold of sorts is crossed at PAH concentrations of a few percent or higher, since it is at this point that the aromatic CH stretching bands first become weakly apparent. However, insofar as they can be recovered by subtraction of nearby H_2O absorption, there is no evidence suggesting the strengths, positions, or widths of these features alter with concentration. At concentrations in excess of a few percent they simply become strong enough to begin to be seen against the strong $3\ \mu m$ H_2O ice feature.

As mentioned earlier, higher concentrations increase the strength of the dangling O-H bands in the 3750 – $3600\ cm^{-1}$ (2.67 – $2.78\ \mu m$) range and can cause their profiles to change, but these are not PAH-specific absorption features and do not constitute a good PAH tracer.

3.4. The Effects of Temperature on the Spectra of H_2O -PAH Ices

In the case of the H_2O /pyrene ≈ 380 and H_2O /perylene ≈ 40 samples, additional spectra were taken of the samples as they were warmed sequentially from their deposition temperature of 15 K to 25, 50, 75, 100, 125, 150, and 175 K. We observed spectral

behaviors that are largely similar to those seen during warm-up sequences with H_2O -naphthalene ices described in greater detail in SBA04. The various pyrene and perylene bands show no major changes in position, width, or relative strength as the samples are warmed from 15 to 125 K, although the perylene peaks showed a steadily increasing, monotonic redshift of $\sim 1.5\ cm^{-1}$ spanning the entire 15–125 K range. Both the pyrene and perylene features show linear redshifts in position as the temperatures go from 125 to 150 to 175 K, with total 125–175 K shifts between being $\sim 2\ cm^{-1}$ in the 2000 – $1000\ cm^{-1}$ range and $\sim 10\ cm^{-1}$ in the 1000 – $500\ cm^{-1}$ range for pyrene, and $\sim 1\ cm^{-1}$ in the 2000 – $1000\ cm^{-1}$ range and $\sim 3\ cm^{-1}$ in the 1000 – $500\ cm^{-1}$ range for perylene. This differs slightly from the naphthalene case, where the shifts were observed to vary from band to band and to be $\leq 2.5\ cm^{-1}$ in *either* direction.

The most noticeable difference is that the pyrene and perylene bands show no splitting and little or no narrowing at 150 and 175 K, whereas most naphthalene bands showed one or both in fairly dramatic fashion at these temperatures. In the H_2O -naphthalene ices, these changes were interpreted as being driven by the H_2O phase transformation from amorphous to cubic ice above 125 K (see SBA04 for a more detailed discussion). The difference in behavior of pyrene and perylene at 150 and 175 K are therefore presumably due to their different sizes; each will be accommodated by the cubic crystalline ice structure differently (i.e., each will substitute for different numbers of H_2O molecules and may preferentially orient in a different size geometry). This suggests that different PAHs might be expected to show a range of different behaviors in band positions, widths, and profiles when in H_2O ices at these temperatures.

It should be noted that, while the (modest) spectral changes that occur during the amorphous to cubic ice transition near 125 K are diagnostic of the H_2O -PAH interaction and H_2O ice structure, they are of limited relevance to the ISM. Since H_2O -rich ices sublime rapidly above 125 K (Sandford & Allamandola 1993); it is unlikely that PAHs frozen in warm ($T > 125\ K$) H_2O -rich ices are abundant in the interstellar medium.

4. ASTROPHYSICAL IMPLICATIONS

These data have a number of potentially important implications for the interpretation of infrared spectra taken along lines of sight that pass through dense cloud materials. These implications will be discussed in considerable detail elsewhere (L. J. Allamandola et al. 2006, in preparation), but a few main points are summarized below.

4.1. The C-H Stretching Region

As is the case with gas-phase PAHs and related materials, the C-H stretching region of H_2O -PAH mixtures does not provide a good means for the identification of specific molecular species, but only classes of species, since all the aromatic and aliphatic CH stretching modes overlap in their characteristic but limited spectral region. This has the compensating advantage, however, that this same limited spectral region can, in principle, be used to provide an assessment of the total column density of aromatic and aliphatic CH bonds along a given line of sight. This, in turn, is a measure of the distribution of cosmic carbon in these important organic classes.

Our earlier work (SBA04) and the work presented here demonstrate that it will be difficult to take advantage of the aromatic CH stretching features to assess total aromatic CH column densities, since the presence of the strong, nearby $3\ \mu m$ H_2O ice feature results in significant suppression of the spectral contrast of the

features. As a result, at the H₂O/PAH ratios currently indicated for dense clouds (Smith et al. 1989; Sellgren et al. 1995; Brooke et al. 1999; Chiar et al. 2000; Bregman et al. 2000; Sandford et al. 2004), it is very difficult to establish unique baselines under these features. This difficulty is mitigated for the aliphatic CH stretching bands produced by H_n-PAHs, however, which are intrinsically stronger per CH bond and fall farther from the 3 μm H₂O feature.

The aliphatic CH stretches of H_n-PAHs are of additional interest in that they may be able to help account for the “red wing” frequently seen on the 3 μm H₂O ice band in many dense clouds (e.g., Smith et al. 1989). This red wing is seen in many protostellar spectra, its extent is very similar to that spanned by the aromatic and aliphatic CH stretches in our H_n-PAH spectra, and the astronomical data may indicate the presence of spectral structure, particularly in the vicinity of the aliphatic CH stretching region near 3.4 μm.

On the basis of laboratory irradiation experiments, H_n-PAHs are expected to be produced whenever normal PAHs are irradiated in H₂O-rich ices (Bernstein et al. 1999, 2002, 2003). They should therefore be present in dense cloud ices and have been observed in the Orion Bar (Sloan et al. 1997). The CH stretching bands of H_n-PAHs isolated in argon matrices show a large degree of variability within the normal aliphatic CH stretching region. This variability is dependent on the degree of excess H atom coverage and the specific location of the excess H atoms. This, in conjunction with the similar spectral behavior of PAHs and H_n-PAHs in H₂O matrices (i.e., the bands get broader but do not shift greatly in position for both PAHs and H_n-PAHs), suggests that mixtures of H_n-PAHs, particularly those with minor excess H coverage, in H₂O ices could produce a blended feature in this spectral region that might account for a significant portion of the “red wing” seen in the 3 μm band in dense cloud spectra.

For example, one can compare the ratio of the depths of the aliphatic CH stretching and 3 μm H₂O features produced by our H₂O/9,10-dihydroanthracene sample to the optical depths at these same positions in the spectra of the objects with red wings discussed by Smith et al. (1989). Such comparisons suggest that over half the absorption in this region could potentially be accounted for by the presence of only a percent or two of H_n-PAHs relative to H₂O, provided the mixture of H_n-PAHs consisted of species with low excess H coverage (exactly the type of H_n-PAHs that would be anticipated if they were manufactured by the photolysis of PAH in H₂O-rich ices; see Bernstein et al. 1999). A more quantitative discussion of this possibility will be presented in a future paper.

4.2. The Use of Argon-isolated PAH Spectra to Interpret Dense Cloud Spectra

Comparisons of the infrared spectra of all the PAHs and related species that we have studied in H₂O matrices (the work shown here and in SBA04) with the spectra of the same molecules in inert argon matrices show a relative uniformity in spectral response. In all cases the presence of H₂O-PAH and PAH-PAH interactions results in only minor changes in band positions ($\Delta\nu < 10 \text{ cm}^{-1}$), increased widths for most bands (FWHM typically $< 10 \text{ cm}^{-1}$, with occasional bands as wide as 25 cm^{-1}), and changes of less than a factor of 1–3 in relative band strengths. These changes are fairly modest and indicate that it should be possible to use the current, more extensive databases of infrared spectra of argon-isolated PAHs isolated to assist with the interpretation of dense cloud spectra that contain potential PAH absorption features. In other words, initial interpretation of PAH absorption features in dense cloud spectra should not require a comparably large H₂O-

PAH spectral database; preliminary work can be done based on the current Ar-PAH database.

However, the variation in relative band strengths by factors of up to 1–3 between features seen in H₂O and argon matrices suggests that the use of the Ar-PAH data will likely not yield column densities to better than this factor. Improved column densities will require comparison to the spectra of relevant H₂O-PAH samples. However, determination of the needed laboratory experiments could wait until comparisons with the Ar-PAH data implicate particular species or subclasses of species.

Again, a more detailed discussion concerning the use of these data to interpret dense cloud spectra will be presented in a forthcoming paper (L. J. Allamandola, S. A. Sandford, & M. P. Bernstein 2006, in preparation).

5. CONCLUSIONS

Polycyclic aromatic hydrocarbons (PAHs) are expected to be present in dense interstellar clouds where they will largely be seen in *absorption*. We have extended our previous work on the infrared spectral properties of the small PAH naphthalene (C₁₀H₈) in several media to include the full mid-infrared laboratory spectra of 11 other PAHs and related aromatic species frozen in H₂O ices: 1,2-dihydronaphthalene (C₁₀H₁₀), anthracene (C₁₄H₁₀), 9,10-dihydroanthracene (C₁₄H₁₂), phenanthrene (C₁₄H₁₀), pyrene (C₁₆H₁₀), benzo[e]pyrene (C₂₀H₁₂), perylene (C₂₀H₁₂), benzo(k)fluoranthene (C₂₀H₁₂), pentacene (C₂₂H₁₄), benzo[ghi]perylene (C₂₂H₁₂), and coronene (C₂₄H₁₂).

These results demonstrate that PAHs and related molecules, as a group, show the same sorts of spectral behaviors as naphthalene when incorporated into H₂O-rich matrices. The absorption bands produced by the aromatic species in H₂O matrices are typically broader (factors of 3–10), show small position shifts in either direction (usually $< 4 \text{ cm}^{-1}$, always $< 10 \text{ cm}^{-1}$), and show variable changes in relative band strengths (typically factors of 1–3) when compared to the same molecules isolated in inert matrices (e.g., Ar or N₂). There is no evidence of systematic increases or decreases in the absolute strengths of the bands of these molecules when they are incorporated in H₂O matrices. In H₂O-rich ices, the absorption bands of these molecules are relatively insensitive to concentration over the range of $10 < \text{H}_2\text{O}/\text{PAH} < 200$. The absorption bands are also insensitive to temperature over the $10 \text{ K} < T < 125 \text{ K}$ range, although the spectra can show dramatic changes as the ices are warmed through the temperature range in which amorphous H₂O ice converts to its cubic and hexagonal crystalline forms ($T > 125 \text{ K}$).

As is the case with gas-phase PAHs and related materials, the C-H stretching region of H₂O-PAH mixtures does not provide a good means for the identification of specific molecular species or classes of species, since all the aromatic and aliphatic CH stretching modes overlap in a limited spectral region. This same limited spectral region can, however, be used to provide an assessment of the total column density of aromatic and aliphatic CH bonds along a given line of sight. Taking advantage of this possibility is difficult, however, since the presence of the strong, nearby 3 μm H₂O ice feature results in significant suppression of the spectral contrast of the CH stretching features, particularly those due to aromatic CH. This difficulty is mitigated somewhat for the aliphatic CH stretching bands produced by H_n-PAHs, which are intrinsically stronger per CH bond and fall farther from the 3 μm H₂O feature.

Given the small observed band shifts caused by H₂O, the current database of spectra from Ar matrix-isolated PAHs and related molecules should be useful for the preliminary search for

these species in dense clouds on the basis of observed absorption band positions. Furthermore, these data permit determination of column densities to better than a factor of 3 for PAHs in dense clouds. Column density determination of detected aromatics to better than a factor of 3 will, however, require good knowledge about the nature of the matrix in which the PAH is embedded and laboratory studies of relevant samples.

This work was fully supported by NASA's Origins of Solar Systems (grant 344-37-1S), Exobiology (grant 344-58-2B), Astrobiology (grant 344-53-1A), and Planetary Geology and Geophysics (grant 344-30-1B) programs. We gratefully acknowledge useful discussions with Charles Bauschlicher and the expert technical and experimental support of Robert Walker. This paper benefited from a helpful review by Perry Gerakines.

REFERENCES

- Allamandola, L. J., Hudgins, D. M., & Sandford, S. A. 1999, *ApJ*, 511, L115
 Allamandola, L. J., & Sandford, S. A. 1988, in *Dust in the Universe*, ed. M. E. Bailey & D. A. Williams (Cambridge: Cambridge Univ. Press), 229
 Allamandola, L. J., Tielens, A. G. G. M., & Barker, J. R. 1989, *ApJS*, 71, 733
 Bauschlicher, Jr., C. W., & Langhoff, S. R. 1997, *Spectrochim. Acta A*, 53, 1225
 Behringer, R. E. 1958, *J. Chem. Phys.*, 29, 537
 Bernstein, M. P., Elsila, J. E., Dworkin, J. P., Sandford, S. A., Allamandola, L. J., & Zare, R. N. 2002, *ApJ*, 576, 1115
 Bernstein, M. P., Mattioda, A. L., Sandford, S. A., & Hudgins, D. M. 2005, *ApJ*, 626, 909
 Bernstein, M. P., Moore, M. H., Elsila, J. E., Sandford, S. A., Allamandola, L. J., & Zare, R. N. 2003, *ApJ*, 582, L25
 Bernstein, M. P., Sandford, S. A., & Allamandola, L. J. 1996, *ApJ*, 472, L127
 Bernstein, M. P., Sandford, S. A., Allamandola, L. J., Chang, S., & Scharberg, M. A. 1995, *ApJ*, 454, 327
 Bernstein, M. P., Sandford, S. A., Allamandola, L. J., Gillette, J. S., Clemett, S. J., & Zare, R. N. 1999, *Science*, 283, 1135
 Bregman, J. D., Hayward, T. L., & Sloan, G. C. 2000, *ApJ*, 544, L75
 Brooke, T. Y., Sellgren, K., & Geballe, T. R. 1999, *ApJ*, 517, 883
 Chiar, J. E., Tielens, A. G. G. M., Whittet, D. C. B., Schutte, W. A., Boogert, A. C. A., Lutz, D., van Dishoeck, E. F., & Bernstein, M. P. 2000, *ApJ*, 537, 749
 Dartois, E., Schutte, W., Geballe, T. R., Demyk, K., Ehrenfreund, P., & d'Hendecourt, L. 1999, *A&A*, 342, L32
 Ehrenfreund, P., & Charnley, S. B. 2000, *ARA&A*, 38, 427
 Ehrenfreund, P., Dartois, E., Demyk, K., & d'Hendecourt, L. 1998, *A&A*, 339, L17
 Gerakines, P. A., et al. 1999, *ApJ*, 522, 357
 Hudgins, D. M., & Allamandola, L. J. 1995a, *J. Phys. Chem.*, 99, 3033
 ———. 1995b, *J. Phys. Chem.*, 99, 8978
 Hudgins, D. M., & Sandford, S. A. 1998a, *J. Phys. Chem.*, 102, 329
 ———. 1998b, *J. Phys. Chem.*, 102, 344
 ———. 1998c, *J. Phys. Chem.*, 102, 353
 Hudgins, D. M., Sandford, S. A., Allamandola, L. J., & Tielens, A. G. G. M. 1993, *ApJS*, 86, 713
 Jenniskens, P., & Blake, D. F. 1994, *Science*, 265, 753
 Jenniskens, P., Blake, D. F., Wilson, M. A., & Pohorille, A. 1995, *ApJ*, 455, 389
 Langhoff, S. R. 1996, *J. Phys. Chem.*, 100, 2819
 Mattioda, A. L., Hudgins, D. M., Bauschlicher, Jr., C. W., Rosi, M., & Allamandola, L. J. 2003, *J. Phys. Chem.*, 107, 1486
 Peeters, E., Hony, S., van Kerckhoven, C., Tielens, A. G. G. M., Allamandola, L. J., Hudgins, D. M., & Bauschlicher, C. W. 2002, *A&A*, 390, 1089
 Rowland, B., & Devlin, J. P. 1991, *J. Chem. Phys.*, 94, 812
 Rowland, B., Fisher, M., & Devlin, J. P. 1991, *J. Chem. Phys.*, 95, 1378
 Sandford, S. A. 1996, *Meteoritics Planet. Sci.*, 31, 449
 ———. 2002, *Planet. Space Sci.*, 50, 1145
 Sandford, S. A., & Allamandola, L. J. 1993, *ApJ*, 417, 815
 Sandford, S. A., Allamandola, L. J., Tielens, A. G. G. M., & Valero, G. J. 1988, *ApJ*, 329, 498
 Sandford, S. A., Bernstein, M. P., & Allamandola, L. J. 2004, *ApJ*, 607, 346 (SBA04)
 Sellgren, K., Brooke, T. Y., Smith, R. G., & Geballe, T. R. 1995, *ApJ*, 449, L69
 Sloan, G., Bregman, J., Geballe, T., Allamandola, L., & Woodward, C. 1997, *ApJ*, 474, 735
 Smith, R. G., Sellgren, K., & Tokunaga, A. T. 1989, *ApJ*, 344, 413
 Szczepanski, J., Wehlburg, C., & Vala, M. 1995, *Chem. Phys. Lett.*, 232, 221
 van Dishoeck, E. 2004, *ARA&A*, 42, 119